New Generation UV-A Filters: Understanding their Photodynamics on a Human Skin Mimic

Temitope T Abiola, Natércia D N Rodrigues, Ho Casey, Daniel J L Coxon, Michael D Horbury, Josene M Toldo, Mariana T Do Casal, Benjamin Rioux, Cédric Peyrot, Matthieu M Mention, et al.

New Generation UV-A Filters: Understanding their Photodynamics on a Human Skin Mimic

Temitope T. Abiola,[†] *Natércia d. N. Rodrigues,*[†] *Ho Casey,*[†] *Daniel J. L. Coxon,* [†,‡,¶] *Michael D. Horbury,*[∫] *Josene M. Toldo,*[ϕ] *Mariana T. do Casal,*[ϕ] *Benjamin Rioux,*[§] *Cédric Peyrot,*[§] *Matthieu M. Mention,*[§] *Patrick Balaguer,*[ʔ] *Mario Barbatti,*[ϕ,*] *Florent Allais,*[§,*] *and Vasilios G. Stavros*[†,*]

† Department of Chemistry, and ‡Department of Physics, University of Warwick, Gibbet Hill Road, Coventry, CV4 7AL

¶ EPSRC Centre for Doctoral Training in Diamond Science and Technology, United Kingdom

∫ School of Electrical and Electronic Engineering, University of Leeds, Leeds, LS2 9JT

ϕ Aix Marseille University, CNRS, ICR, Marseille, France.

§ URD Agro-Biotechnologies Industrielles (ABI), CEBB, AgroParis Tech, 51110, Pomacle, France

ʔ IRCM, Inserm, Univ. Montpellier, ICM, Montpellier, France.

CORRESPONDING AUTHORS

* v.stavros@warwick.ac.uk *mario.barbatti@univ-amu.fr *florent.allais@agroparistech.fr

ABSTRACT

The sparsity of efficient commercial ultraviolet-A (UV-A) filters is a major challenge towards developing effective broadband sunscreens with minimal human- and eco-toxicity. To combat this, we have designed a new class of Meldrum-based phenolic UV-A filters. We explore the ultrafast photodynamics of coumaryl Meldrum, CMe, and sinapyl Meldrum, SMe, both in an industry standard emollient and on a synthetic skin mimic, using femtosecond transient electronic and vibrational absorption spectroscopies, and computational simulations. Upon photoexcitation to the lowest excited singlet state (S_1), these Meldrum-based phenolics undergo fast and efficient non-radiative decay to repopulate the electronic ground state (S_0). We propose an initial ultrafast twisted intramolecular charge transfer mechanism as these systems evolve out of the Franck-Condon region towards an S_1/S_0 conical intersection, followed by internal conversion to S_0 and subsequent vibrational cooling. Importantly, we correlate these findings to their long-term photostability upon irradiation with a solar simulator and conclude that these molecules surpass the basic requirements of an industry standard UV filter.

TOC GRAPHICS

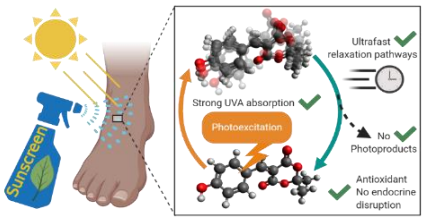

KEYWORDS Ultrafast spectroscopy, sunscreens, nature-inspired, photoprotection, photochemistry, photophysics.

INTRODUCTION

Biological systems rely on solar radiation from the Sun to provide light, warmth and energy to sustain life.[1] However, excessive exposure to ultraviolet (UV) radiation from the Sun at the Earth's surface (UV-B: 280 – 315 nm, UV-A: 315 – 400 nm) causes adverse effects such as tanning (which occurs as a response to photodamage to the skin), sunburn, DNA mutations and photoaging in humans.[2-4] The naturally occurring UV-absorbing pigment in human skin, melanin, often provides insufficient protection against high levels of UV radiation and sunscreens are commonly used for additional photoprotection.[2] While the sunscreen industry has focused on the more energetic UV-B radiation, UV-A is very abundant at the Earth's surface and penetrates deeper into the skin than UV-B.[5,6] Moreover, the adverse effects of overexposure of human skin to UV-A are widely reported to include DNA mutation, pigmentation, suppression of acquired immunity and production of harmful reactive oxygen species in the skin; all of which facilitate carcinogenesis.[5,7] Therefore, photoprotection against UV-A radiation is of crucial importance, but it is hindered by the sparsity of approved commercial UV-A filters, as well as their lack of photostability (*e.g.* avobenzone).[8,9] In addition to being photostable, and blending into a non-toxic and aesthetically pleasing sunscreen formulation, an effective UV-filter within a sunscreen formulation should be able to dissipate the excess energy absorbed safely (*i.e.* without generating photoproducts) and quickly, both to prevent harmful side reactions and to ensure the UV-filter is 'recycled' (i.e. that it returns from the electronic excited state to the electronic ground state without detriment to its molecular integrity), to maintain photoprotection.[2,10]

Recently, the photodynamics of sinapoyl malate (see Figure 1), a natural UV-absorbing compound in *Arabidopsis thaliana*,[11,12] have been reported and found to enable efficient dissipation of absorbed energy in the form of heat, through a proposed *trans*-*cis* isomerization across the allylic bond.[13,14]

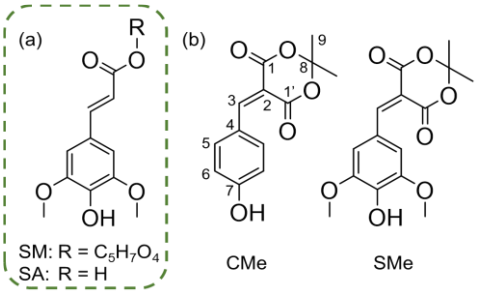

Figure 1. Chemical structure of (a) plant UV-filter in *Arabidopsis thaliana,* sinapoyl malate (SM) and its building block sinapic acid (SA), and (b) coumaryl Meldrum (CMe) and sinapyl Meldrum (SMe) studied herein.

Furthermore, in methyl and ethyl sinapate (where R = CH_3 and C_2H_5 in Figure 1a, respectively), photoexcitation to the lowest excited singlet state (S_1) was found to lead to ultrafast *trans*-*cis* isomerization mediated *via* a conical intersection (CI) between the S_1 state and the electronic ground state (S_0), denoted S_1/S_0 CI.[13,15-18] The same CI that allows a portion of the population to isomerize, leading to the *cis*-isomer, also facilitates repopulation of the original ground state of the *trans*-isomer.[15,16] The *cis*-isomer of related cinnamates has been reported to possess a lower UV absorption (*i.e.* lower extinction coefficient) and, importantly, significantly higher genotoxicity.[19,20] One way to circumvent concerns related to the genotoxicity of potential photoexcitation by-products, such as geometric isomers, is to design UV-filters with identical functional groups around the allylic bond, so that isomerization results in no significant alteration of molecular structure and properties.

An example of such a symmetrically substituted UV-filter is diethyl sinapate (DES), the photodynamics of which were recently investigated.[19] The study showed not only that ground state recovery of DES is very fast, but also that the absorption spectrum of DES is spectrally red shifted (further into the UV-A region) relative to its monoester building block, ethyl sinapate.[19] We have synthesized a new class of symmetrically substituted sinapate esters[21] in an attempt to further enhance UV-A absorption whilst maintaining the efficacy of ground state recovery.

In this work, we present a multi-pronged experimental and computational study to unravel the photodynamics of a novel class of Meldrum-based phenolic UV-A filters inspired by nature, specifically CMe and SMe, shown in Figure 1b and c, respectively. We utilize transient electronic and vibrational spectroscopies to gain unprecedented insight into the electronically excited and ground state dynamics of these UV-A filters. Importantly, we have adapted our experimental setup to ensure that our experiment models the conditions these UV-A filters are found in commercial formulations (dissolved in an emollient) as closely as possible; we have deposited the bulk solution of these UV-A filters (dissolved in an emollient) on a synthetic skin mimic to model the application environment of the sunscreen. This will enable us to discern if the skin surface perturbs the dynamics of the UV-filters. As detailed further in section A of the Supporting Information (SI), we have supplemented these ultrafast experiments with ultraslow experiments, ascertaining the long-term photostability of these UV-filters when exposed to radiation from a solar simulator, as well assessing their endocrine disruption and antioxidant properties. To complement these experiments and to better understand the dynamics of CMe and SMe, we employ high-level calculations. These reveal a new relaxation mechanism in these plant-derived UV filters involving a twisted intramolecular charge transfer state that allows the photoexcited molecule to return to its electronic ground state with exceptionally high efficiency.

RESULTS

Experimental Findings

Steady-state UV-vis absorption spectra were obtained for separate solutions of CMe and SMe in the industry standard emollient caprylic capric triglyceride (CCT) and in ethanol. As shown in Figure 2 and SI section B, the absorption maxima (λ_{max}) are located at 362 nm for CMe in CCT (denoted CMe/CCT, similarly for SMe, and in all other solutions henceforth) and 375 nm for CMe/ethanol. In the case of SMe/CCT and SMe/ethanol, λ_{max} is located at 396 nm and 407 nm, respectively. The molar extinction coefficient of CMe and SMe at their λ_{max} are 29,877 and 32,105 $mol^{-1}dm^3cm^{-1}$, respectively, which is comparable to that of the globally most common UV-A filter, avobenzone, which has a reported molar extinction coefficient of 34,140 $mol^{-1}dm^3cm^{-1}$.[22]

We investigated the long-term photostability of CMe and SMe in CCT, as shown in Figure 2, by collecting UV-vis spectra at various time-intervals after irradiation with a solar simulator. These measurements revealed that CMe and SMe in CCT experience only a minor reduction in absorbance of less than 10% over an irradiation period of two hours. Equivalent photostability tests could not be performed for CMe/CCT or SMe/CCT deposited on synthetic skin mimic (VITRO-CORNEUM®, VC) due to excessive scattering from the sample precluding any reliable measurements. For the transient electronic absorption spectroscopy (TEAS) presented in the results section, we have modified our experimental setup by increasing the pump-probe incidence angle to minimize this scattering and use off-axis parabolic mirrors to enhance collection of scattered transmitted light (see SI, section A).

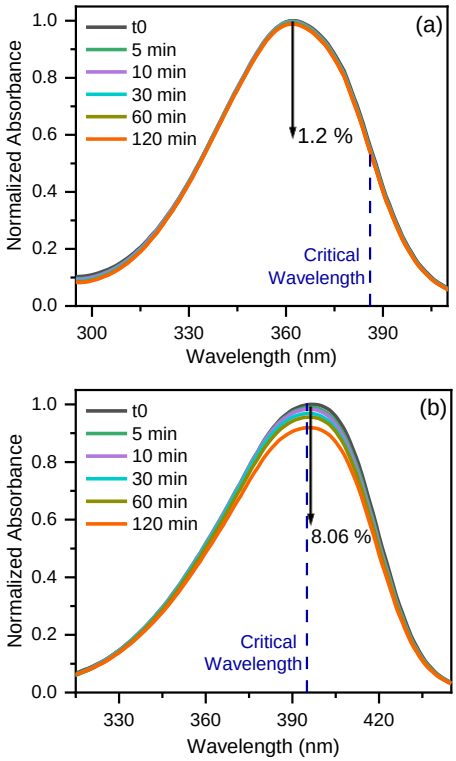

Figure 2. Photostability of (a) CMe and (b) SMe in CCT recorded at different intervals during irradiation with a solar simulator. The vertical dashed lines on each panel represent the position of the calculated critical wavelength of 384 nm and 395 nm for CMe and SMe, respectively.

In addition to photostability tests, the critical wavelengths (CW) of CMe and SMe were determined from their corresponding UV-vis spectra; these values are shown as a vertical dashed lines in Figure 2a,b. The CW of a UV-filter is defined as the wavelength at which the integrated area under the spectral absorbance curve reaches 90% of the total area between 290 and 400 nm.[23] The concept of CW in UV-A protection has been widely reported in previous literature.[23-25] To be labelled as broadband spectrum protection in the USA, a sunscreen must have a CW of at least 370 nm. The CW of CMe/CCT and CMe/ethanol were determined to be 384 nm and 395 nm, respectively (SI Figure S2); for SMe/CCT and SMe/ethanol, the CW takes values of 395 nm and 396 nm, respectively (cf. 378 nm for avobenzone in ethanol[19]). Furthermore, endocrine disruption

analysis was conducted for SMe and reported in the SI, section D, to supplement those already reported for CMe;[21] both molecules are found to be innocuous in this sense.

To elucidate the origin of the photostability of CMe and SMe, we investigated their ultrafast (femto- to pico-seconds) photodynamics with TEAS. A full description of our experimental setup and procedures are detailed in the SI, section A. TEAS measurements obtained for separate solutions of CMe/CCT, SMe/CCT, CMe/ethanol and SMe/ethanol are presented in the SI, in Figure S4 and S5, and discussed in SI section E. Presented in Figure 3 are the TEAS measurements for separate solutions of CMe/CCT and SMe/CCT at 20 mM deposited on VC (denoted CMe VC/CCT and SMe VC/CCT). The transient electronic absorption (TEA) spectra of CMe and SMe are, in all environments (CCT, ethanol and VC), dominated by four features: first, there is a negative feature centred at ~362 nm for CMe and ~396 nm for SMe, attributed to a ground state bleach (GSB) through comparison with the steady-state UV-vis absorption spectra (see Figure 2a,b); a second, negative feature centred at ~450 nm and ~475 nm in CMe and SMe, respectively, is attributed to stimulated emission (SE) between the S_1 ($1^1\pi\pi^*$) state and the S_0 state, based on our electronic structure calculations (discussed below) and the emission spectra presented in SI section F. We note, for the purpose of the discussion below, that the SE feature observed for CMe appears to decay back to baseline within ~1 ps, while that of SMe persists up to ~5 ps. Thirdly, there is an intense positive feature attributed to excited state absorption (ESA) of the S_1 ($1^1\pi\pi^*$) state, centred at ~365 nm in both CMe and SMe; finally, close examination of the TEA spectra of both molecules reveals a second ESA centred at ~420 nm, which decays on a similar timescale to the GSB and is more clearly visible in the evolution associated difference spectra (EADS) in Figure 3 and SI Figure S4. We suggest that this ESA feature results from the formation of vibrationally hot electronic ground state following internal conversion from S_1 to S_0 mediated by the S_1/S_0 CI.

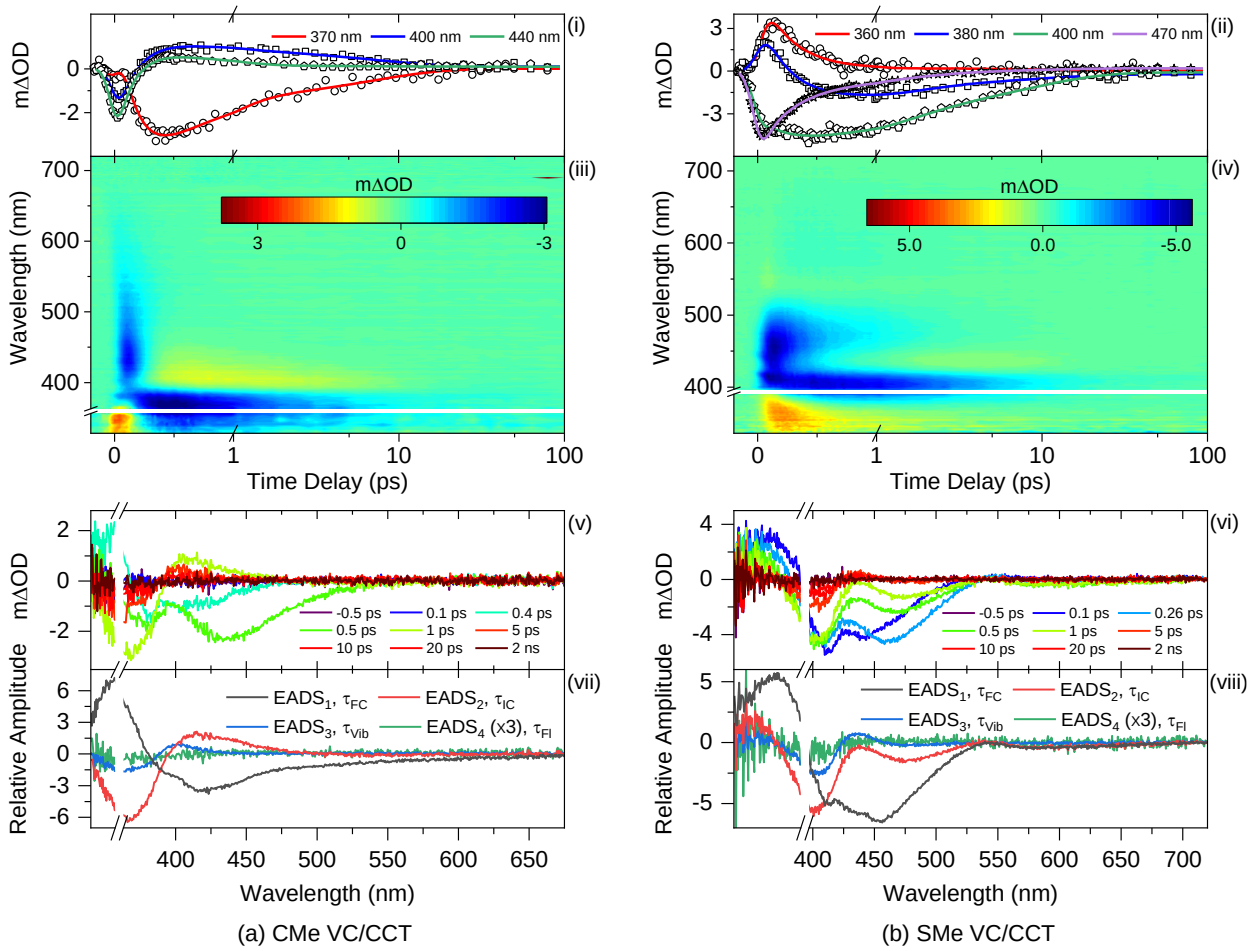

Figure 3. TEA spectra obtained for 20 mM (a) CMe VC/CCT photoexcited at 362 nm, and (b) SMe VC/CCT photoexcited at 396 nm. The TEA spectra are presented as false color maps in panel (iii) and (iv), respectively. The same data is presented as a line plots of mΔOD *vs* probe wavelength at selected pump-probe time delays in panels (v) and (vi). The top panels (i) and (ii) show transients (raw data as symbol and fits as solid lines) at selected probe wavelengths. The bottom panels (vii) and (viii) show the EADS produced by the fitting procedure (see main text for details), $EADS_4$ is multiplied by three as a visual aid. The masked region of the TEA spectra, line plots and EADS of CMe VC/CCT and SMe VC/CCT corresponds to the wavelengths for which excess scatter from the pump pulse (caused by the uneven surface of VC) interferes with data subtraction and renders the data void.

To extract kinetic information from the TEA spectra, we carried out global fitting employing a sequential ($A \overset{\tau_1}{\rightarrow} B \overset{\tau_2}{\rightarrow} C \overset{\tau_3}{\rightarrow} D\ldots$) kinetic model using the Glotaran software package.[26,27] The extracted time-constants τ_n (where n denotes the dynamical process associated with each time-constant) are shown in Table 1. The errors quoted for these fits are those produced by the fitting software; however, the quality of each fit is best evaluated by analysis of the associated residuals shown in SI section G (Figure S7). The solvent only time-zero responses, which correspond to our instrument response, are shown in Figure S8 discussed in SI section H.

Table 1. Summary of the time-constants and associated errors extracted from data collected for CMe and SMe in CCT, VC/CCT and ethanol with TEAS, TVAS, and theory in implicit ethanol.

		TEAS			**TVAS**	**Theory**
		CCT (1 mM)	VC/CCT (20 mM)	Ethanol (1 mM)	Ethanol (30 mM)	Implicit ethanol
CMe	τ_{FC} / fs	220 ± 40	190 ± 40	190 ± 40	1240 ± 20	334 ± 12[a]
	τ_{IC} / fs	460 ± 40	450 ± 40	450 ± 40	–	628 ± 56[a]
	τ_{Vib} / ps	10.02 ± 0.22	6.92 ± 0.26	7.78 ± 0.13	7.44 ± 0.61	–
	τ_{Fl} / ns	–	>2	–	>1.5	–
SMe	τ_{FC} / fs	300 ± 40	280 ± 40	350 ± 40	–	~600[b]
	τ_{IC} / ps	1.15 ± 0.04	1.21 ± 0.05	0.79 ± 0.04	–	~0.94[b]
	τ_{Vib} / ps	8.26 ± 0.04	8.69 ± 0.43	4.26 ± 0.09	5.06 ± 0.08	–
	τ_{Fl} / ns	>2	>2	>2	>1.5	5.7[c]

[a] dynamics simulations of 70 trajectories. [b] dynamics of 10 trajectories. [c] first-order perturbation theory. τ_{FC} corresponds to the time to relax from the Franck-Condon (FC) to the twisted CT minimum, τ_{IC} is the S_1/S_0 internal conversion time, τ_{Vib} is the time for vibrational cooling in the ground state, and τ_{Fl} is the fluorescence time for a minor fraction of the population that does not undergo IC. TEA spectra time-constants under other conditions are given in SI, Table S1.

Complementary transient vibrational absorption spectroscopy (TVAS) measurements, *i.e.* UV-pump/infrared(IR)-probe, were obtained for CMe and SMe in order to probe changes in vibrational state on the S_0 electronic surface following internal conversion from the S_1 state. Due to the strong IR absorption of CCT, TVAS measurements were taken in ethanol, which we have found from

TEAS measurements presented in SI section E to be comparable to a CCT environment. The transient vibrational absorption (TVA) spectra for CMe and SMe are reported in Figure 4 (see SI Figure S9 for additional TVA spectra and section I for discussion). The strongest GSB features observed in the TVA spectra of CMe and SMe were fitted with tri-exponential (CMe) and bi-exponential (SMe) functions, shown in Figure 4, yielding the time-constants, shown in Table 1. The fit of the GSB feature at 1510 cm^{-1} for CMe and 1558 cm^{-1} for SMe, as well as the GSB feature at 1714 cm^{-1} (reported in SI Figure S9) for both UV-filters are reported in SI Table S2.

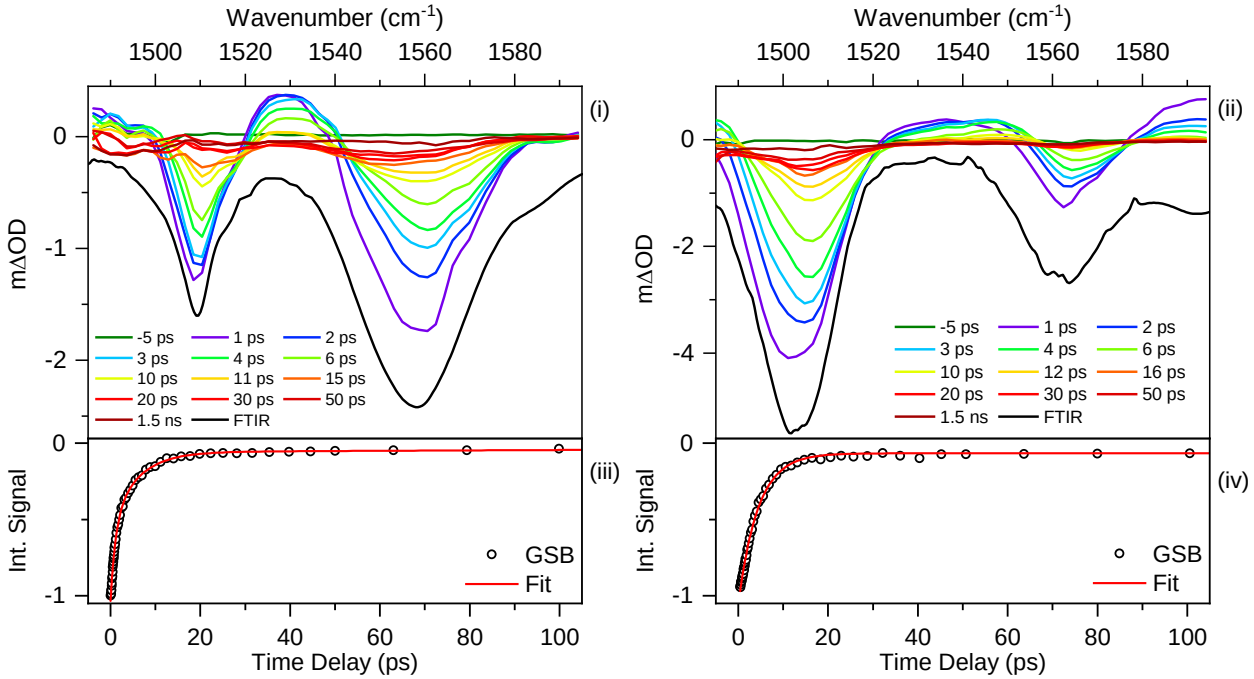

Figure 4. TVA spectra obtained for 30 mM solution of (a) CMe/ethanol following 375 nm excitation, and (b) SMe/ethanol following 407 nm excitation, using a probe pulse centred at 1536 cm^{-1}. The TVA spectra are presented as smoothed line plots of mΔOD vs probe wavenumber at selected pump-probe time delays in panels (i) and (ii) respectively. The steady-state Fourier transform infrared (FTIR) spectra of CMe/ethanol and SMe/ethanol are shown as black lines in panels (i) and (ii). The bottom panels (iii) and (iv) show the transients for the GSB recovery (raw

data as open circles and fit as solid red line) of signals at selected wavenumber. For CMe/ethanol the normalized integration of the 1558 cm^{-1} GSB signal was fitted with a tri-exponential function, while the normalized integration of the 1505 cm^{-1} GSB signal was fitted with a bi-exponential function for SMe/ethanol. Attempt to fit CMe/ethanol data with a bi-exponential function returned a poor fit. Frequency calculations (see SI section J) suggest the vibrational feature probed is the allylic C=C stretching at 1558 cm^{-1} and aromatic C-H bending and C=C stretching at 1505 cm^{-1}.

Computational Studies of CMe and SMe

In interpreting experimental results, we have made use of electronic structure calculations (details in SI section J) carried out for CMe and SMe using an implicit solvation model for ethanol. The inclusion of explicit solvation does not have significant effect on the vertical excitations, although it slightly stabilizes the lowest ππ* states and destabilizes the lowest nπ* state (see Tables S3 and S4 in the SI). Optimized geometries are shown in SI Figure S10, along with the initial excitation in Figures S11 and S12. In addition, molecular orbital characterization for the singlet states is shown in Figure S13 and S14. The calculated vertical excitations presented in Table 2 show that photoexcitation at λ_{max} of CMe and SMe corresponds to population of the bright S_1 state ($1^1\pi\pi^*$). For CMe, this state has a large oscillator strength and lies below the $^1n\pi^*$ state (S_3 state) by 0.9 eV, according to the TD-ωB97XD and CASPT2 results (see SI Table S3). This energy difference is slightly greater for SMe (1.1 eV) due to stabilization of the ππ* states arising from the electron donor methoxy groups.

Following the vertical excitation, the optimization of the S_1 ($1^1\pi\pi^*$), S_2 ($2^1\pi\pi^*$), and S_3 ($1^1n\pi^*$) states shows that the $1^1\pi\pi^*$state is largely stabilized, lying below the nπ* state by ~1.8 eV for both molecules (see the adiabatic energies in Table 2). This large energy difference between the states hinders any possibility of internal conversion to a dark $^1n\pi^*$ state, previously reported as a

competitive decay channel for other cinnamate and sinapate derivatives.[12,28,29] The strong stabilization of the S_1 state occurs through twisting around the C2-C3 (see Figure 1) allylic bond towards a twisted intramolecular charge transfer (TICT) minimum, $S_{1\text{-TICT}}$, at $\phi \sim 90°$ twist (state characterization is given in SI Table S5; ϕ is the C1'-C2-C3-C4 dihedral angle).

Table 2. Vertical absorption energy into S_n (ΔE_{vert}), vertical emission energy (ΔE_{em}), and adiabatic energy (ΔE_{adiab}) for CMe and SMe, calculated with TD-DFT (ωB97XD/aug-cc-pVDZ//ωB97XD/cc-pVDZ; PCM (ethanol)). Oscillator strengths are given in the parentheses.

		ΔE_{vert} / eV		**ΔE_{em} / eV**		**ΔE_{ad} / eV**	
CMe	S_1	ππ*	3.83 (0.8765) 3.31[a]	ππ*	0.79 (0.0000)	ππ*	2.51 (0.0000)
	S_2	ππ*	4.62 (0.0074)	nπ*	3.14 (0.0321)	ππ*	4.25 (0.0511)
	S_3	nπ*	4.70 (0.0038)	ππ*	3.64 (0.0244)	nπ*	4.30 (0.0160)
SMe	$S_{1\text{-LE}}$	ππ*	3.57 (0.6662) 3.05[a]	ππ*	2.77 (0.5281)	ππ*	3.18 (0.5281)
	$S_{1\text{-TICT}}$		--	ππ*	0.82 (0.0000)	ππ*	2.49 (0.0000)
	S_2	ππ*	3.86 (0.0183)	ππ*	2.76 (0.0168) [b]		NO[c]
	S_3	nπ*	4.68 (0.0019)	nπ*	3.14 (0.0968) [b]	nπ*	4.29 (0.0000)

[a] Experimental values in ethanol. [b] Relative to $S_{1\text{-TICT}}$ minimum. [c] NO: Not obtained; the state optimizes to $S_{1\text{-FC}}$.

The excited-state topography of SMe and CMe revealed by the theoretical approach is schematically shown in Figure 5. While CMe shows a barrierless S_1 relaxation towards the $S_{1\text{-TICT}}$ twisted minimum, in SMe the equivalent relaxation leads to a flat region on the potential energy surface (PES), with a locally excited minimum ($S_{1\text{-LE}}$) and partially twisted geometry ($\phi \sim 40°$). The barrier between the TICT and LE minima is less than 0.1 eV (see SI Figure S15 and S16).

Near the 90° twisted geometry, a S_1/S_0 minimum energy crossing point was found 0.2 eV (at TD-DFT) above the $S_{1\text{-TICT}}$ minimum for both CMe and SMe (SI Figure S16). This up-hill intersection was determined for both molecules using TD-DFT and further confirmed by CASPT2//CASSCF calculations for CMe, which provided a 0.37 eV barrier.

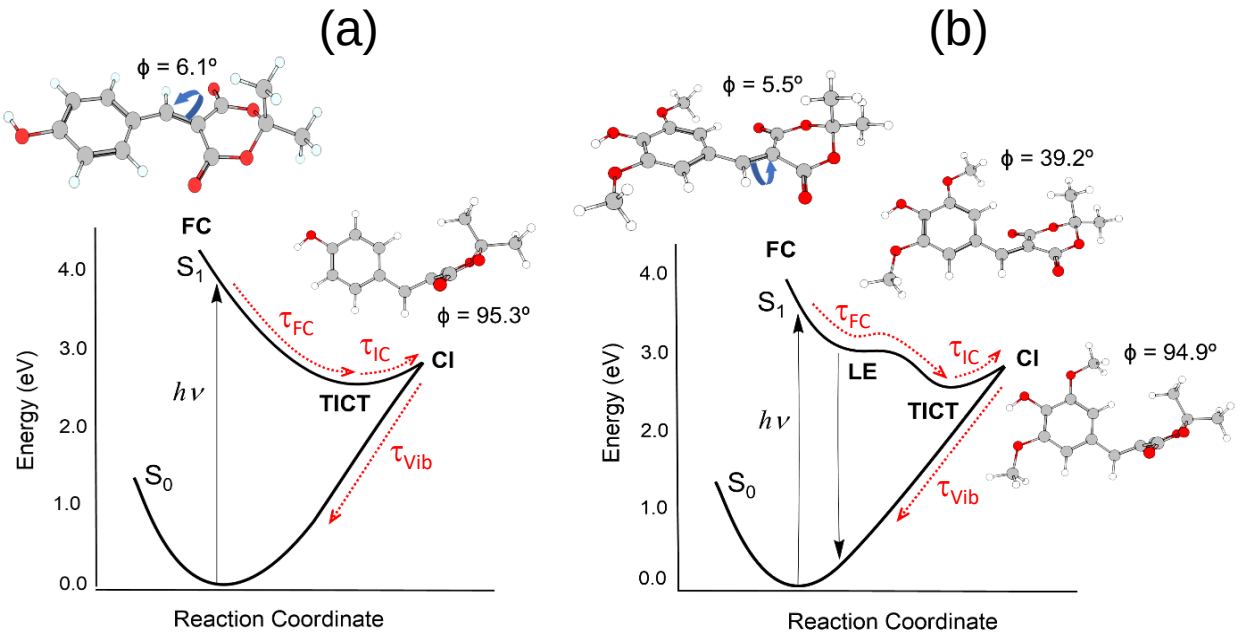

Figure 5. Topography of the PES for CMe (left) and SMe (right). Minima and state intersections calculated with TD-DFT at ωB97XD/aug-cc-pVTZ//ωB97XD/cc-pVDZ level with implicit ethanol solvent, the solid lines schematically interpolate these points. Molecular conformations at the Franck-Condon (FC) region, at the global minimum ($S_{1\text{-TICT}}$) and at the local $S_{1\text{-LE}}$ minimum (only for SMe) are shown. Their twisting angles ϕ (C1'-C2-C3-C4 dihedral angle) are also indicated. The molecular structures for the S_1/S_0 intersection are omitted here for clarity but are shown in Figure S15; they are qualitatively similar to the $S_{1\text{-TICT}}$ with twisting angle ϕ = 94.8° and ϕ = 86.8° for CMe and SMe, respectively.

To verify the time evolution of the molecules along this pathway, we performed excited-state dynamics simulations by propagating an ensemble of trajectories using TD-DFT (ωB97XD/cc-pVDZ) in implicit ethanol until S_1 reached a crossing with S_0 (see SI section J-iii). The time to reach the crossing point for each trajectory was assumed to correspond to the internal conversion (IC) time. For CMe, all trajectories undergo an ultrafast twist around the allylic bond, which drives it towards the intersection with the ground state. Monitoring the dynamics starting from the vertically excited-state, we have observed that the S_1/S_0 energy gap quickly drops to ~0.5 eV with a mean time of 334 ± 12 fs, when twisted geometries near 90° are reached (SI Figure S19), in good agreement with the experimental τ_{FC} (see Table 1). After this gap closure, the molecule requires a further 300 fs to reach the S_1/S_0 intersection which, as we mentioned, is energetically above the $S_{1\text{-TICT}}$ minimum. During this time, the S_1/S_0 energy gap remains small (<0.5 eV) and we can observe oscillations in bond lengths, ring puckering and pyramidalization of the C3 atom (see Figure 1). The IC follows an exponential decay pattern with a mean time of 628 ± 56 fs, in line with the experimentally obtained τ_{IC} (see Table 1). For SMe, only a few trajectories with exploratory character and low statistical significance were run. For this molecule, the dynamics evolution is similar, although it is elongated to ~600 fs due to the flat region around the $S_{1\text{-LE}}$ minimum. Like in CMe, IC takes a further 300 fs, occurring at ~940 fs.

DISCUSSION

We now discuss the implications of our results with regards to photoprotection, drawing on the different aspect of the experimental and computational studies. The presented UV-vis spectra, photostability and CW tests reveal that CMe and SMe are photostable UV-A absorbers. In addition, previous studies have reported not only promising antioxidant properties for this class of molecules,[21] but also lack of endocrine disruption effect for the CMe.[21] Endocrine disruption

analysis for SMe highlighted the same innocuousness (see SI section D). Together, these observations make CMe and SMe promising candidates for inclusion in commercial formulations,[19] although further analysis of their toxicity is needed. With regards to their ultrafast photodynamics, which should allow for fast and efficient dissipation of excess energy, we draw on our experimental results, calculations, and previous related studies to assign dynamical processes to extracted time-constants and to discuss the implications of our findings.

Previous studies on related systems have shown that, following initial photoexcitation to the $1^1\pi\pi^*$ state, these molecules tend to undergo rapid geometry and vibrational relaxation out of the Franck-Condon region, usually evidenced by slight changes in the EADS.[13,16,19] While we might expect CMe and SMe to undergo a similar dynamical process, the EADS associated with τ_{FC} ($EADS_1$) is significantly different from $EADS_2$ (see Figure 3). This marked difference suggests either a change of state or excited-state population migration to a drastically different region of the PES. Indeed, our calculations reveal that the relaxation of the initially excited $1^1\pi\pi^*$ state of both CMe and SMe follows a large energy stabilization alongside a marked geometrical change. As indicated in Figure 5, the $1^1\pi\pi^*$ state evolves into a global minimum with a geometry twisted ~90° around the allylic double bond and large charge-transfer character prior to reaching a CI with the ground state. TICT processes have been previously reported for systems in which electron withdrawing and donating substituents are positioned para to each other (i.e. position 1 and 4 on the benzene ring), lending further support to our hypothesis.[30-32] Hence, we assign τ_{FC} for CMe and SMe (see Table 1), to an ultrafast relaxation into the TICT minimum ($S_{1\text{-TICT}}$). Once this minimum is reached, we propose that IC takes place from the TICT to the ground state within the timescale of τ_{IC}. These assignments of τ_{FC} and τ_{IC} are confirmed by the results of our excited-state

dynamic simulations, which yield times for movement out of the Franck-Condon region that are in excellent agreement with experimental τ_{FC} value (see Table 1).

In addition, the time constants associated with the recovery of GSB features in the TVA spectra effectively correspond to the rate of vibrational cooling of the vibrationally hot S_0, as previously described for other systems.[33,34] The first time-constant (~1 ps) extracted from the fit to each GSB feature of the TVA spectra in CMe, as well as the GSB feature of SMe at 1714 cm^{-1}, encompasses several initial processes, including solvent heating and any overlapping features. Consequently, we refrain from conclusive assignment of this time constant in these cases. However, τ_{Vib} for CMe and SMe from their TVA spectra match the equivalent τ_{Vib} values in TEA spectra in ethanol (see Table 1): τ_{Vib} ~8 ps observed for CMe in TVA spectra and TEA spectra, and τ_{Vib} ~5 ps in TVA spectra and ~4 ps in TEA spectra for SMe. This agreement confirms our assignment of τ_{Vib} for CMe and SMe in TEA spectra (in both ethanol and CCT) to vibrational cooling within their respective S_0 states.

Finally, the remaining time-constant extracted from the TVA spectra, τ_{Fl}, is associated with the residual GSB feature observable in the EADS of both CMe and SMe. This feature persists beyond the 2 ns temporal window of our experiments, with < 1% of the feature's intensity remaining (see SI Figure S20). The linear power dependence observed for these measurements (see SI section L, Figure S21) suggests that it does not correspond to radical formation, which has previously been attributed to a two-photon ionization mechanism.[13,35] We address this incomplete recovery of the ground state by once again considering the results of our electronic structure calculations: as discussed, the only difference between the potential energy profiles of CMe and SMe is the partially-twisted LE minimum in the S_1 state of SMe. Although this minimum has a small energy barrier (<0.1 eV), we show in SI section J-iv that a small fraction of the SMe population could be

trapped in the S1-LE minimum long enough to fluoresce at 448 nm emission, within 5.7 ns (in reasonable agreement with the TEAS result in ethanol, 475 nm in > 2 ns). We note, however, that the absence of a SE feature beyond 5 ps and up to 2 ns in the TEA spectra could simply reflect the small amount of trapped population in the S_1-LE state, leading to a weak SE that is within the signal-to-noise of the TEA spectra. For CMe, although we do not observe S_1-LE minimum on the PES, a small fraction of the population could be trapped within the shallow TICT minimum or some other state not captured by our calculation, which could explain the incomplete recovery of the GSB feature in EADS4, clearly visible in the 2 ns TEA spectrum in the SI (Figure S20). An alternative relaxation pathway for the long-lived species (represented by τ_{Fl}) could be intersystem crossing (ISC) from the S_1 to triplet state. However, we are unable to confirm or rule out either mechanism; the weak fluorescence emission from CMe and SMe has precluded us from ascertaining any reasonable fluorescence lifetime measurements. Independently of the τ_{Fl} assignment, it is crucial to note that additional TEAS measurements, NMR and HPLC measurements presented in SI Figure S22, S23 and S24 lead us to confidently conclude that the long-lived τ_{Fl} is not likely to be the result of interaction with the skin mimic, nor is it associated with the formation of any potentially harmful photoproduct in either CMe or SMe.

In summary, combining ultrafast transient absorption spectroscopy, excited-state calculations, and steady-state studies, we have provided unprecedented insight into the excited-state photodynamics of CMe and SMe in closer-to-real environments (i.e. in industrial grade emollient and on skin mimic surface, providing more than just conventional solvent-chromophore interaction). Following photoexcitation of CMe and SMe to their respective S_1 states (in either bulk ethanol, CCT, or deposited on a skin mimic), our results reveal fast relaxation involving TICT followed by IC to the S_0 state and vibrational cooling on the ground state surface. Finally, we note

a mild incomplete ground state recovery within 2 ns, which we assigned to excited-state population trapped at a locally excited minimum. Steady-state studies revealed that these molecules are highly photostable over prolonged irradiation, surpassing the most widely used UV-A filter on the market (avobenzone). These studies also demonstrate that these filters do not produce any observable photoproducts after two hours of simulated solar irradiation (see SI section M). Importantly, our results showed that the dynamics of CMe and SMe are, at best, mildly influenced by environment following our studies in ethanol, emollient and on a skin mimic. Allied to the strong UV-A protection they afford and the favorable antioxidant and endocrine disruption tests,[21] CMe and SMe present as highly promising candidates for inclusion in commercial sunscreen formulations.

Given the importance of structure-dynamics-function relationships in a multitude of fields, including the present studies linked to sunscreen science, our work clearly demonstrates that the dynamics of CMe and SMe UV-filters are only mildly influenced by surrounding environment (solution versus skin mimic). Coupled to the demonstration that symmetrical substitution across the allylic bond circumvents the formation of potentially toxic geometric isomer photoproducts, our nature-inspired UV-filters offer a promising avenue of photon-to-molecule heat generation. This has ramifications, not just to researchers within the sunscreen industry, but researchers whose work targets, more broadly, photon-to-molecule energy conversion such as light capturing for solar fuels, light driven catalyst for fine chemicals and fluorophores with environment specific emission for medical imaging.

ASSOCIATED CONTENT

Supporting Information.

The Supporting Information is available free of charge in PDF.

Experimental methods, photostability measurements of CMe and SMe in ethanol, critical wavelength of CMe and SMe in ethanol, endocrine disruption measurements of SMe, additional TEAS measurements of CMe/CCT, SMe/CCT, CMe/ethanol and SMe/ethanol at 1 mM concentration, emission spectra of CMe and SMe in ethanol, residuals between fits returned by sequential fit and raw data for CMe and SMe in CCT and VC/CCT, instrument response, TVAS experimental setup and additional data, pump power dependence study, TEAS measurements of CMe/CCT and SMe/CCT at higher concentration, ^{1}H NMR of pre- and post-irradiated CMe and SMe, HPLC chromatogram of pre- and post-irradiated CMe and SMe on VC, kinetic fits. Computational details: further description of methodology, vertical and adiabatic energies at different levels of theory, optimized structures, representative trajectories, analysis of fluorescence in SMe.

AUTHOR INFORMATION

Notes

The authors declare no competing financial interests.

ACKNOWLEDGMENT

The authors thank the support of the FetOpen grant BoostCrop (Grant agreement 828753). The authors would like to thank the Warwick Centre for Ultrafast Spectroscopy (WCUS) for the use of transient vibrational absorption spectroscopy (TVAS) and Fluorolog 3. T.T.A thanks The

University of Warwick for PhD studentship through the Chancellor Scholarship. M.D.H thanks the Leverhulme Trust for postdoctoral funding. M.T do C, J.M.T, and M.B thank the project Equip@Meso (ANR-10-EQPX-29-01) funded by the French Government "Investissements d'Avenir" program for the computational resources. B.R, C.P, M.M.M and F.A thank the Agence Nationale de la Recherche (grant number ANR-17-CE07-0046), as well as the Grand Reims, Conseil Départemental de la Marne, and the Grand Est region for financial support. V.G.S thanks the Royal Society and Leverhulme Trust for a Royal Society Leverhulme Trust Senior Research Fellowship. The authors thank Nikola Chmel, Abbigail Whittock and Michael Staniforth for their help and useful discussion.

REFERENCES

1. Ahmed, F. K.; Lim, H. W.; Draelos, Z. D., Worldwide regulation of UV filters: current status and future trends. In *Clinical guide to sunscreens and photoprotection*, Informa Healthcare, New York: 2009; pp 65-81.
2. Baker, L. A.; Marchetti, B.; Karsili, T. N. V.; Stavros, V. G.; Ashfold, M. N. R., Photoprotection: extending lessons learned from studying natural sunscreens to the design of artificial sunscreen constituents. *Chem. Soc. Rev.* **2017,** *46* (12), 3770-3791.
3. Rodrigues, N. D. N.; Cole-Filipiak, N. C.; Horbury, M. D.; Staniforth, M.; Karsili, T. N. V.; Peperstraete, Y.; Stavros, V. G., Photophysics of the sunscreen ingredient menthyl anthranilate and its precursor methyl anthranilate: A bottom-up approach to photoprotection. *J. Photochem. Photobiol., A* **2018,** *353*, 376-384.
4. Dahle, J.; Kvam, E., Induction of delayed mutations and chromosomal instability in fibroblasts after UVA-, UVB-, and X-radiation. *Cancer Res.* **2003,** *63* (7), 1464-1469.
5. Battie, C.; Jitsukawa, S.; Bernerd, F.; Del Bino, S.; Marionnet, C.; Verschoore, M., New insights in photoaging, UVA induced damage and skin types. *Exp. Dermatol.* **2014,** *23*, 7-12.
6. Brenner, M.; Hearing, V., The protective role of melanin against UV damage in human skin. *Photochem. Photobiol.* **2008,** *84* (3), 539-549.
7. Matsumura, Y.; Ananthaswamy, H. N., Molecular mechanisms of photocarcinogenesis. *Front. Biosci.* **2002,** *7*, d765-83.
8. Afonso, S.; Horita, K.; e Silva, J. P. S.; Almeida, I. F.; Amaral, M. H.; Lobão, P. A.; Costa, P. C.; Miranda, M. S.; da Silva, J. C. G. E.; Lobo, J. M. S., Photodegradation of avobenzone: stabilization effect of antioxidants. *J. Photochem. Photobiol., B* **2014,** *140*, 36-40.
9. Mturi, G. J.; Martincigh, B. S., Photostability of the sunscreening agent 4-tert-butyl-4′-methoxydibenzoylmethane (avobenzone) in solvents of different polarity and proticity. *J. Photochem. Photobiol., A* **2008,** *200* (2-3), 410-420.

10. Rodrigues, N. D. N.; Staniforth, M.; Stavros, V. G., Photophysics of sunscreen molecules in the gas phase: a stepwise approach towards understanding and developing next-generation sunscreens. *Proc. R. Soc. A* **2016,** *472* (2195), 20160677.
11. Fraser, C. M.; Chapple, C., The phenylpropanoid pathway in Arabidopsis. *The Arabidopsis Book/American Society of Plant Biologists* **2011,** *9*.
12. Dean, J. C.; Kusaka, R.; Walsh, P. S.; Allais, F.; Zwier, T. S., Plant sunscreens in the UV-B: ultraviolet spectroscopy of jet-cooled sinapoyl malate, sinapic acid, and sinapate ester derivatives. *J. Am. Chem. Soc.* **2014,** *136* (42), 14780-14795.
13. Baker, L. A.; Horbury, M. D.; Greenough, S. E.; Allais, F.; Walsh, P. S.; Habershon, S.; Stavros, V. G., Ultrafast photoprotecting sunscreens in natural plants. *J. Phys. Chem. Lett.* **2015,** *7* (1), 56-61.
14. Luo, J.; Liu, Y.; Yang, S.; Flourat, A. L.; Allais, F.; Han, K., Ultrafast barrierless photoisomerization and strong ultraviolet absorption of photoproducts in plant sunscreens. *J. Phys. Chem. Lett.* **2017,** *8* (5), 1025-1030.
15. Baker, L. A.; Staniforth, M.; Flourat, A. L.; Allais, F.; Stavros, V. G., Gas-Solution Phase Transient Absorption Study of the Plant Sunscreen Derivative Methyl Sinapate. *ChemPhotoChem* **2018,** *2* (8), 743-748.
16. Horbury, M. D.; Flourat, A. L.; Greenough, S. E.; Allais, F.; Stavros, V. G., Investigating isomer specific photoprotection in a model plant sunscreen. *Chem. Commun.* **2018,** *54* (8), 936-939.
17. Horbury, M. D.; Quan, W.-D.; Flourat, A. L.; Allais, F.; Stavros, V. G., Elucidating nuclear motions in a plant sunscreen during photoisomerization through solvent viscosity effects. *Phys. Chem. Chem. Phys.* **2017,** *19* (31), 21127-21131.
18. Zhao, X.; Luo, J.; Liu, Y.; Pandey, P.; Yang, S.; Wei, D.; Han, K., Substitution Dependent Ultrafast Ultraviolet Energy Dissipation Mechanisms of Plant Sunscreens. *J. Phys. Chem. Lett.* **2019,** *10*, 5244-5249.
19. Horbury, M. D.; Holt, E. L.; Mouterde, L. M. M.; Balaguer, P.; Cebrián, J.; Blasco, L.; Allais, F.; Stavros, V. G., Towards symmetry driven and nature inspired UV filter design. *Nat. Commun.* **2019,** *10* (1), 1-8.
20. Sharma, A.; Bányiová, K.; Babica, P.; El Yamani, N.; Collins, A. R.; Čupr, P., Different DNA damage response of cis and trans isomers of commonly used UV filter after the exposure on adult human liver stem cells and human lymphoblastoid cells. *Sci. Total Environ.* **2017,** *593*, 18-26.
21. Peyrot, C.; Mention, M. M.; Brunissen, F.; Balaguer, P.; Allais, F., Innovative Bio-Based Organic UV-A and Blue Light Filters from Meldrum's Acid. *Molecules* **2020,** *25* (9), 2178.
22. Shaath, N. A., Ultraviolet filters. *Photochem. Photobiol. Sci.* **2010,** *9* (4), 464-469.
23. Diffey, B., A method for broad spectrum classification of sunscreens. *Int. J. Cosmet. Sci.* **1994,** *16* (2), 47-52.
24. Wang, S. Q.; Xu, H.; Stanfield, J. W.; Osterwalder, U.; Herzog, B., Comparison of ultraviolet A light protection standards in the United States and European Union through in vitro measurements of commercially available sunscreens. *J. Am. Acad. Dermatol.* **2017,** *77* (1), 42-47.
25. Diffey, B., The FDA final rule on labeling and effectiveness testing of sunscreens: Too little, too late? *J. Am. Acad. Dermatol.* **2012,** *66* (1), 162-163.
26. Snellenburg, J.; Laptenok, S.; Seger, R.; Mullen, K.; Van Stokkum, I., Glotaran: A Java-based graphical user interface for the R package TIMP. *J. Stat. Softw.* **2012**, 49.

27. Mullen, K. M.; Van Stokkum, I. H. M., TIMP: an R package for modeling multi-way spectroscopic measurements. *J. Stat. Softw.* **2007,** *18* (3), 1-46.
28. Tan, E. M. M.; Amirjalayer, S.; Bakker, B. H.; Buma, W. J., Excited state dynamics of Photoactive Yellow Protein chromophores elucidated by high-resolution spectroscopy and ab initio calculations. *Faraday Discuss.* **2013,** *163* (0), 321-340.
29. Kinoshita, S.-n.; Inokuchi, Y.; Onitsuka, Y.; Kohguchi, H.; Akai, N.; Shiraogawa, T.; Ehara, M.; Yamazaki, K.; Harabuchi, Y.; Maeda, S.; Ebata, T., The direct observation of the doorway 1nπ* state of methylcinnamate and hydrogen-bonding effects on the photochemistry of cinnamate-based sunscreens. *Phys. Chem. Chem. Phys.* **2019,** *21* (36), 19755-19763.
30. Rodrigues, N. D. N.; Cole-Filipiak, N. C.; Turner, M. A.; Krokidi, K.; Thornton, G. L.; Richings, G. W.; Hine, N. D. M.; Stavros, V. G., Substituent position effects on sunscreen photodynamics: A closer look at methyl anthranilate. *Chem. Phys.* **2018,** *515*, 596-602.
31. Weersink, R. A.; Wallace, S. C., Complexes of Methyl 4-(N, N-Dimethylamino) benzoate: Spectroscopy and Dynamics of the Charge Transfer State. *J. Phys. Chem.* **1994,** *98* (42), 10710-10719.
32. Howell, R.; Phillips, D.; Petek, H.; Yoshihara, K., Fluorescence of jet-cooled dimethylamino benzonitrile, its aggregates and solvated complexes. *Chem. Phys.* **1994,** *188* (2-3), 303-316.
33. Baker, L. A.; Horbury, M. D.; Greenough, S. E.; Coulter, P. M.; Karsili, T. N. V.; Roberts, G. M.; Orr-Ewing, A. J.; Ashfold, M. N. R.; Stavros, V. G., Probing the ultrafast energy dissipation mechanism of the sunscreen oxybenzone after UVA irradiation. *J. Phys. Chem. Lett.* **2015,** *6* (8), 1363-1368.
34. Roberts, G. M.; Marroux, H. J. B.; Grubb, M. P.; Ashfold, M. N. R.; Orr-Ewing, A. J., On the participation of photoinduced N–H bond fission in aqueous adenine at 266 and 220 nm: a combined ultrafast transient electronic and vibrational absorption spectroscopy study. *J. Phys. Chem. A* **2014,** *118* (47), 11211-11225.
35. Horbury, M. D.; Baker, L. A.; Rodrigues, N. D. N.; Quan, W.-D.; Stavros, V. G., Photoisomerization of ethyl ferulate: A solution phase transient absorption study. *Chem. Phys. Lett.* **2017,** *673*, 62-67.